Interferometric characterization of rotation stages for X-ray nanotomography

Tomaš Stankevič, Christer Engblom, Florent Langlois, Filipe Alves, Alain Lestrade, Nicolas Jobert, Gilles Cauchon, Ulrich Vogt, and Stefan Kubsky

Citation: Review of Scientific Instruments **88**, 053703 (2017); doi: 10.1063/1.4983405
View online: http://dx.doi.org/10.1063/1.4983405
View Table of Contents: http://aip.scitation.org/toc/rsi/88/5
Published by the American Institute of Physics

REVIEW OF SCIENTIFIC INSTRUMENTS **88**, 053703 (2017)

Interferometric characterization of rotation stages for X-ray nanotomography

Tomaš Stankevič,[1] Christer Engblom,[2] Florent Langlois,[2] Filipe Alves,[2] Alain Lestrade,[2] Nicolas Jobert,[2] Gilles Cauchon,[2] Ulrich Vogt,[3] and Stefan Kubsky[2]
[1]*MAX IV Laboratory, Lund University, P.O. Box 118, SE-221 00 Lund, Sweden*
[2]*Synchrotron SOLEIL, L'Orme des Merisiers, Saint-Aubin BP48, 91192 Gif-sur-Yvette, France*
[3]*Biomedical and X-Ray Physics, KTH/Royal Institute of Technology, KTH-AlbaNova, SE-106 91 Stockholm, Sweden*

(Received 19 December 2016; accepted 1 May 2017; published online 16 May 2017)

The field of three-dimensional multi-modal X-ray nanoimaging relies not only on high-brilliance X-rays but also on high-precision mechanics and position metrology. Currently available state-of-the-art linear and rotary drives can provide 3D position accuracy within tens to hundreds of nm, which is often insufficient for high resolution imaging with nanofocused X-ray beams. Motion errors are especially troublesome in the case of rotation drives and their correction is more complicated and relies on the metrology grade reference objects. Here we present a method which allows the characterisation and correction of the radial and angular errors of the rotary drives without the need for a highly accurate metrology object. The method is based on multi-probe error separation using fiber-laser interferometry and uses a standard cylindrical sample holder as a reference. The obtained runout and shape measurements are then used to perform the position corrections using additional drives. We demonstrate the results of the characterization for a piezo-driven small rotation stage. The error separation allowed us to measure the axis runout to be approximately ±1.25 μm, and with active runout compensation this could be reduced down to ±42 nm. *Published by AIP Publishing.* [http://dx.doi.org/10.1063/1.4983405]

I. INTRODUCTION

Scanning x-ray microscopy techniques have become standard tools to image both natural and man-made samples with nanometer (nm) resolution in three-dimension.[1,2] X-rays allow us to image a range of material properties, such as distributions of electron density, elemental and chemical compositions, crystal structures, magnetization, and strain.[3–6] Thanks to the short wavelength of x-rays and recent advancements in developments of x-ray focusing optics, focal spots smaller than 10 nm can be produced for scanning image techniques.[7] Further improvements of resolution can be achieved using lensless coherent imaging methods, such as ptychography.[8] However, as in any type of imaging, the resolution ultimately depends on the stability and positioning accuracy of the sample with respect to the X-ray beam.[9] Three-dimensional volumetric images are produced using tomographic techniques from a range of 2D projections. The quality and resolution of the reconstruction is directly dependent on the precise alignment of these projections. Since the target resolution is in the range of nm, the accuracy and precision of the sample translation and rotation drive have to be of the same order. Unfortunately, most of the commercially available rotation and translation drives cannot fulfill such requirements due to the excessive crosstalk, axis runout, and wobble.[10]

A work-around solution to fix the misalignment of the 2D projections that occurs due to the rotation errors is to re-align them in post-processing using known high contrast reference points on the sample.[11] However, this requires an additional data processing step which takes time and can reduce the data quality. Moreover, not all samples can be equipped with clear reference marks. The preferred way is to ensure that the sample is at known positions during the measurement by the characterization and compensation of the positioning errors using additional drives during the measurements. This principle has been employed by a number of modern X-ray nanoimaging beamlines at different synchrotron radiation facilities.[11–14] By keeping the rotation axis in place during the whole scan, the recorded projections are aligned during acquisition and no additional data manipulations are needed.

Several successful implementations of feedback systems to measure and compensate for the rotational errors during nano-tomography scans have been realized using high accuracy metrology objects.[11–15] This resulted in achieving a dramatic increase in the 3D image resolution, reaching below 20 nm.[16] However, in all cases the quality of the reference object determines the best achievable resolution. Such reference cylinders or spheres are also expensive and should be handled with care in order to preserve their nm-level surface and shape quality. In this paper, we present a method and a prototype for a rotational sample stage which can be used to obtain nm-level rotation accuracy, not limited by the quality of the reference cylinder.[17]

II. EXPERIMENTAL SETUP

The scanning x-ray tomography sample stage presented in this paper consists of a stack of translation drives for the sample scanning in three orthogonal directions, rotation around a vertical axis, and additional drives for the sample alignment with the rotation axis. The drawing of the sample stage is

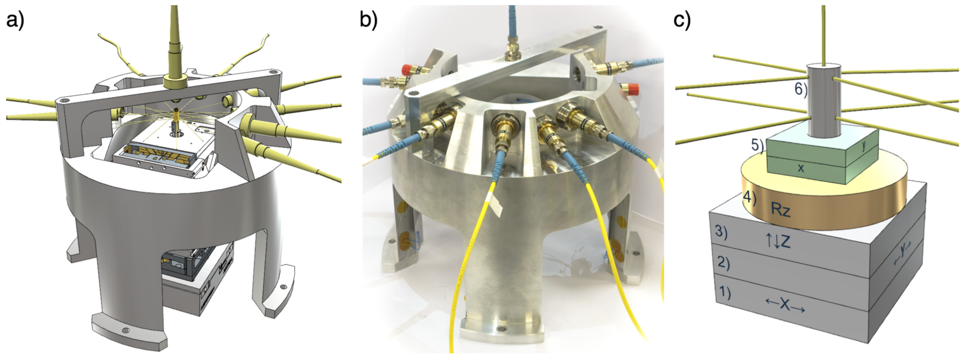

FIG. 1. (a) Drawing of the sample stage with the interferometric characterization setup. The outer frame serves as a support for the interferometer objectives, whereas the actual sample stage can be seen underneath. Up to ten interferometers can be pointed at the reference cylinder from different directions to measure axial runout, radial runout, and wobble of the rotation axis. Moreover, the system allows for characterization of linear drives (linearity, crosstalk, and tilt). (b) A photo of the setup. (c) Schematic diagram of the sample stage, consisting of the three orthogonal linear drives at the bottom: (1) Magnetic linear drive for fast continuous scanning, (2) multi-feet piezo linear drive for sample positioning along the X-ray beam, (3) multi-feet piezo linear drive for step-scanning in vertical direction, (4) stick-slip piezo rotation drive, (5) sample alignment drives (stick-slip), and (6) brass reference cylinder. The yellow lines represent the interferometry beams pointing at the side surfaces of the reference cylinder at two different levels as well as from the top.

shown together with the interferometric characterization bench in Fig. 1(a). A functional layout of the different sample stages is schematically illustrated in Fig. 1(c). The bottom linear drive (Aerotech ANT95-L) is meant for continuous fast scanning in the horizontal direction X, perpendicular to the x-ray beam (1). Above it is the multi-feet piezo drive PI LPS-65 for sample positioning along the beam Y (2). The same type of linear multi-feet piezo drive is used for vertical sample scanning along Z (3). Next is the compact stick-slip piezo rotational drive Rz (Xeryon XRTA) for the rotation of the sample around the Z axis. Finally, two orthogonal linear piezo stages (x, y) are used to align the rotation axis with the reference cylinder (6) and the sample on top of it. All translation and rotation drives were controlled by a Delta Tau PowerPMAC motion controller in order to perform coordinated motions.

The drawing and the photo of the interferometric characterization bench are shown in Figs. 1(a) and 1(b). It comprises an aluminum frame hosting ten interferometer channels (Attocube FPS3010): nine of them are distributed around the reference pin and one is pointing from the top. The interferometry fibers are attached to custom focusing objectives with a variable focal length. The objective heads are adjusted so that the focus of the laser beam is close to the surface of the reference cylinder. The tilts of all objective heads are adjusted in order to maximize the signal using the flexible hinge mounts between the heads and the mounting frame. The top-view interferometer uses a collimated 1.6 mm laser beam and measures the distance with respect to the flat mirror attached on the top of the reference pin. In order to reduce the effects of thermal expansion during measurements, thermal drifts in the system are stabilized down to 5 mK/h. This is accomplished using a passive water flow through the baseplate below the sample stage and the interferometry reference frame. Air turbulence is reduced by using a plastic enclosure around the setup.

The purpose of the interferometric characterization bench is to characterize the motion errors induced by the rotational and scanning linear drives and to measure the shape of the reference cylinder. The shape of the reference cylinder, the radial runout, and the wobble of the rotation axis are measured using the multi-probe error separation method.[18] For that, 4 interferometry channels, measured at different azimuthal angles during the whole rotation, are used to measure the reference cylinder displacements in the XY plane as a function of the rotation around the Z axis. This allows us to extract the roundness along one circle of the cylinder surface and the axis runout as a function of the rotation angle. In order to measure the angular wobble of the axis, additional 4 interferometers measure the runout at a different height along the cylinder (5 mm above). Having measured the axis runout at 2 different levels along the cylinder axis, it is possible to calculate the angular wobble during the rotation. Two additional interferometry channels are mounted parallel with the linear sample drives (Y and Z) in order to monitor the crosstalk and linearity thereof. Whereas such a large number of interferometers are necessary to obtain the full information about the scanning drives and the reference cylinder, it is impractical to have all of them at the beamline due to space constraints. Therefore, the purpose of such a characterization bench is to pre-characterize the reference cylinder and individual sample stages before they are mounted at the beamline. Once the shape of the reference cylinder and the repeatable motion errors are known, it is sufficient to have only a minimum number of interferometers at the beamline setup for the feedback of non-repeatable motion errors—three channels to compensate for the runout and additional two for the wobble errors.

III. RESULTS

Due to the complex mechanics of the miniature rotation drives, the perfect rotary motion is disturbed by forces from the stick-slip piezoelectric drive elements, the guide bearings, external load, and other factors. The rotary errors are a combination of linear runout in radial and axial directions as well as angular axis wobble. Due to the different nature of the disturbances, they contribute either to synchronous (repeatable after full rotation) or asynchronous (non-repeatable) errors. While the measured synchronous error can be readily used as the feed-forward information to the linear compensation drives, asynchronous errors can only be corrected in a feedback loop, relying on the known shape of the reference surface. Therefore, precise information about the shape of the reference cylinder is critical for the compensation of the asynchronous axis runout and wobble.

The concept, allowing us to obtain resolutions higher than the accuracy of the reference cylinder, relies on the on-site characterization of the reference cylinder in terms of the roundness errors. This can be done using one of the established error separation methods, such as the multi-probe error separation using laser interferometers.[18,19] The method uses three or more laser interferometry probes distributed at fixed azimuth angles around the reference cylinder. The measurement is done by rotating the cylinder around its axis using the rotary drive whilst measuring the displacement of the cylinder surface with respect to each probe. Next, the cylinder shape along the measured circle, as well as the axis runout of the rotary drive at every measurement step, is calculated from the set of linear equations. It has been demonstrated that such a method can be applied to measure axis runout with nm precision.[20] The use of four probes instead of three also allows us to optimize unknown experimental errors, such as determining the true azimuthal angles of the fixed probes, thus greatly reducing the measurement error.

Here we extended this method by performing error separation measurements at two different levels along the cylinder axis. This allows us to calculate the angular wobble of the axis. In the case of thick samples, the angular wobble parallel to the X-ray beam can become a bottleneck in obtaining the nm resolution in 3D tomography, since (as opposed to the sample drifts and tilts perpendicular to the beam) it is not possible to compensate for in post-processing.

A. Radial runout and cylinder shape measurement

Radial runout was measured at two levels of the reference cylinder, separated by 5 mm. 4 interferometers were used at each level, placed at the following azimuthal angles for bottom level: 0°, 55°, 135°, 207°, where 0° is parallel to the X axis. The interferometry heads at the top level were placed at the same intervals but shifted by 20° with respect to the bottom level due to space considerations. Each head was aligned using the flexure hinges, so that all 4 laser beams at each level intersected at the center of the reference cylinder. The cylinder was aligned with respect to the rotation axis using the topmost linear drives (Fig. 1(b)). However, due to the fixed inclination of the cylinder, the eccentricity could be minimized only for one of the two levels. The focal distance was tuned using the objective lenses in order to reduce the spot size on the cylinder surface and assure sufficient intensity of the reflected laser beams. The measurements of the radial runout and the cylinder shape were done by performing a full rotation of the cylinder in 256 steps. At each step, the displacement measurements from all interferometers were taken with 1 s averaging time and 1 s delay for the settling of the motors.

The method for the multi-probe error separation is described in, e.g., Ref. 20. The error separation was performed for the top and bottom levels of the cylinder independently. First, the optimization of the probe (interferometer) angles was done. Due to the mounting and alignment errors, the actual probe angles differed slightly from the nominal positions. Next, the cylinder shape and radial axis runout were calculated from the rotational scans. Fig. 2 shows the raw measurements from 8 interferometers as well as results of the error separation.

From Fig. 2(b), showing the raw measurements from the top and bottom levels, we can see that during a single rotation the measured displacements of the cylinder surface change by approximately ±5 μm at the top level and ±15 μm at the bottom level. The bottom level also contains much stronger contribution of the 1st harmonic, corresponding to the eccentricity, compared to the top level. This is caused by the fact that the eccentricity at the top level was minimized when pre-aligning the cylinder with the linear drives ((5) in Fig. 1(c)). From the results of the error separation, we can see that the shape (Fig. 2(c)) of the cylinder varies in the range of 2 μm. Shape variations between the top and bottom measurements are of the order of few 10s of nanometers. Panel (d) shows the radial axis runout ε during one rotation, projected on x and y axes and shifted for clarity. Black and red curves correspond to the runout measured at the top and bottom levels of the cylinder, respectively. We can see that in both cases the runout reaches up to ±2 μm. Changes of few 100 nm between the top and bottom layers indicate the presence of the axis wobble. By using more than three probes for error separation, the problem was overdetermined, which allowed us to estimate the measurement error. The root mean squared (RMS) error, obtained by comparing the measured and simulated displacement data, was 12 nm. In other words, 90% of the measurement points deviate from the true value by less than ±20 nm.

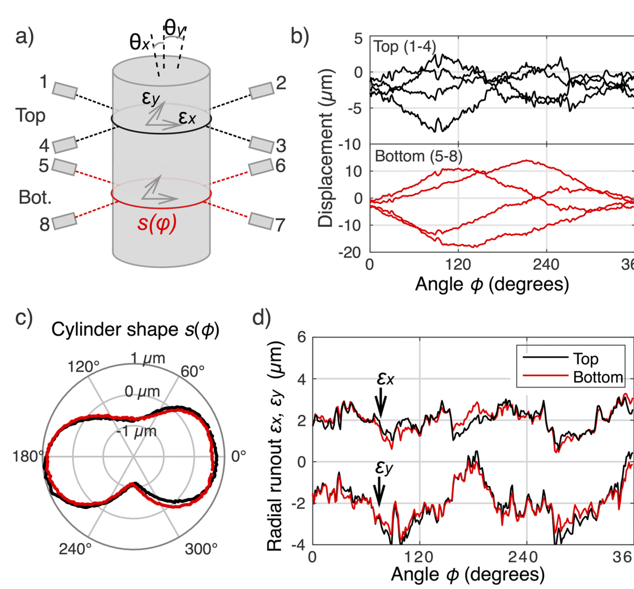

FIG. 2. (a) A sketch of the reference cylinder and the two measurement levels—top and bottom. The cylinder shape $s(\phi)$ and the radial runout $\varepsilon(\phi)$ are measured at both levels independently. (b) Raw measurements taken by all 8 interferometry channels. ((c) and (d)) Results of the error separation. (c) shows the cylinder shape error at the two levels, which varies in the range of 2 μm. (d) The radial runout of the axis along x and y coordinates. The curves are shifted for clarity. The small difference of runout between the top and bottom layers is due to the angular wobble of the rotation axis.

B. Repeatability of runout and wobble

In order to determine the repeatability of the radial axis runout and wobble, we have repeated the measurement, described above, 30 times. Each measurement was done while rotating the stage clockwise and returning it anticlockwise back to the initial position. The average shape of the cylinder after 30 rotations is shown in Fig. 3(a). The standard deviation of the shape based on 30 scans and averaged over 256 points per rotation is 12 nm, which corresponds to the RMS error obtained from the error separation procedure on a single rotation. The average runout along x and y axes is plotted as thick lines in Fig. 3(b). The thin lines show the most extreme deviations from the mean among 30 measurements. This illustrates the repeatability of the rotation errors. Analysis showed that the repeatability is better along the y axis, where the non-repeatable fraction comprises 15% of the mean (repeatable) runout. Along the x axis the repeatability is worse; on average 20% of the mean radial runout along the x direction is non-repeatable. Additionally, the repeatability is worse at the beginning and the end of the range. This can be attributed to an issue with excessive tension of the cables for the uppermost linear drives, which twisted during the scan. The issue was fixed in later measurements.

Having measured the runout at two different levels along the cylinder, separated by 5 mm, it was straightforward to determine the angular wobble of the rotation axis. The result is shown in Fig. 3(c), with the thick lines showing the mean wobble around x and y axes and thin lines representing largest deviations from the mean among 30 scans. We can see that the maximum wobble is slightly beyond ± 100 μrad along both axes. The non-repeatable parts of the wobble components θ_x and θ_y are 24% and 19%, respectively.

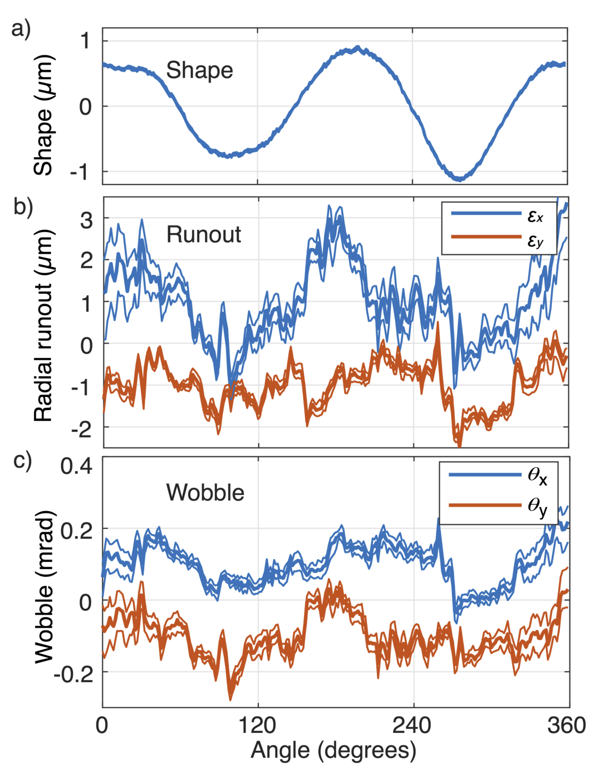

FIG. 3. (a) Average shape error of the reference cylinder after 30 measurements. (b) Radial axis runout averaged over 30 measurements (thick lines). Thin lines correspond to extreme deviations from the mean, which represents the non-repeatable fraction of the runout error. (c) Axis wobble averaged over 30 measurements (thick lines). Similar to (b), thin lines represent extreme deviations from the mean—non-repeatable wobble. Runout and wobble curves along x and y are shifted for clarity.

C. Compensation of repeatable runout errors

Using the mean runout from 30 measurements shown above, we have implemented a look-up table for the feed-forward compensation of the rotation errors using the linear scanner drives X and Y. The compensation table was stored in the Delta Tau motion controller, which was programmed to apply the corresponding compensation movements of the X and Y linear drives as a function of the angular position of the rotational drive. This way the repeatable rotation errors could be corrected without real-time feedback from interferometers.

In order to visualize the effect of the compensation table, we show the x-y scatter plot of the runout and define the circle of confusion, containing 90% of the data points. In Fig. 4(a) we can see the implementation of the compensation scheme using the motion controller and look-up table. Without the active runout correction, the radius of the circle of confusion in the X-Y plane is equal to 1.25 μm (Fig. 4(b)). After the implementation of the feed-forward active compensation, we performed 10 more rotation scans in order to characterize the remaining runout. Just as before, we measured the displacement of the reference surface with interferometers and calculated the axis runout using error separation. However, these measurements were not used for real-time error corrections in any way. The

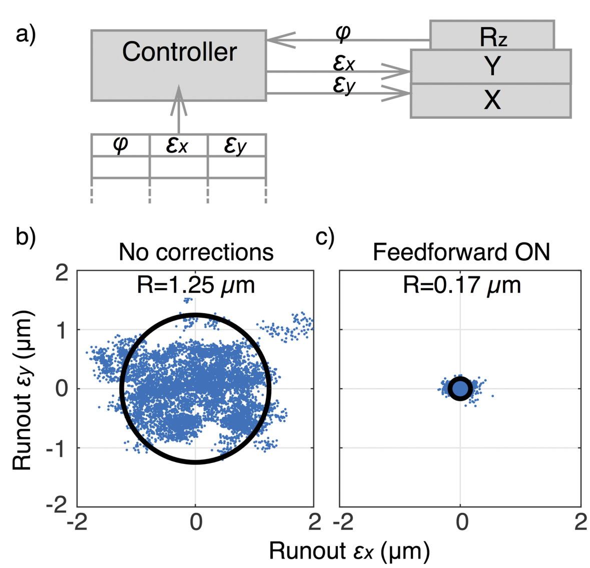

FIG. 4. (a) Motion control scheme using the feed-forward corrections from the look-up table acquired in the earlier step. A fixed offset is applied to the bottom X and Y drives for every angle of the rotation drive Rz. The look-up table contains the mean runout errors averaged over multiple scans, so that they correspond to the repeatable runout. (b) Distribution of the runout points measured during 30 scans, 256 steps each. The radius of the 90% circle of confusion is 1.25 μm. (c) Axis runout measured with active feed-forward compensation during 10 scans of 256 steps. The circle of confusion decreased down to 0.17 μm, since the repeatable part of the axis runout was canceled with the linear drives. The remaining circle of confusion corresponds to the non-repeatable axis runout.

resulting runout error is shown in Fig. 4(c), where it is clearly visible that the circle of confusion is much narrower, reaching only 0.17 μm as opposed to the initial 1.25 μm. The remaining error corresponds to the non-repeatable fraction of the runout and, unfortunately, cannot be compensated by only using the look-up table.

D. Compensation of total rotation runout

In order to compensate for the remaining radial runout errors, we employed an interferometric closed-loop feedback system using only two orthogonal interferometers, parallel with the X and Y linear drives (Fig. 5). As opposed to the runout errors, the shape of the reference cylinder remains constant at every rotation. Therefore, it can be used as the reference for the error compensation. For that, the Delta Tau motion controller was programmed to adjust the position of the linear X and Y drives so that the displacement measured with the interferometers would always follow the cylinder shape profile. The cylinder shape profile was supplied as two look-up tables for two orthogonal interferometry channels: $s(\phi)$ and $s(\phi + 90°)$. Two independently running proportional-integral-derivative (PID) loops were employed for controlling the linear drives X and Y, each taking the shape profile as a set-point for the corresponding interferometry channels. The simplified control scheme is shown in Fig. 5(a). In order to measure the remaining axis runout, we used three additional interferometers that were not used in the real-time feedback but allowed performing the error separation for diagnostics of the performance. The results of the error separation from 2 rotations showed that the remaining radial runout is ±42 nm (Fig. 5(c)), as defined by the radius of the 90% circle of confusion. While the circle of confusion is a more practical definition of the motor accuracy, the standard deviation σ = 13.5 nm shows that the remaining runout is mainly limited by the uncertainty of the error separation routine, which was applied twice in series: first time to determine the pin shape and second time during the final diagnostics of the closed-loop feedback control.

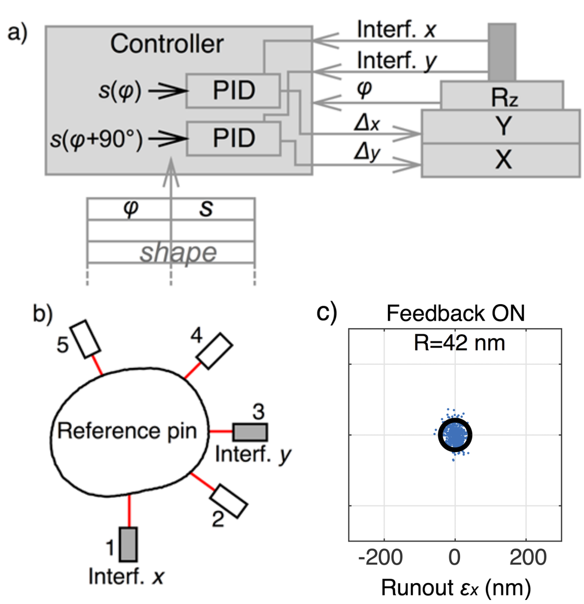

FIG. 5. (a) Motion control scheme using the interferometric feedback from two orthogonal heads and the look-up table containing the previously measured shape of the reference cylinder. The continuous corrections Δx and Δy are applied in a PID loop to the main scanning axes X and Y so that the final displacements measured with interferometry are equal to the pin shape. (b) 2 interferometers heads were used for continuous feedback (1 and 3), while the remaining three interferometers were used for diagnostics and error separation in order to estimate the remaining runout error. (c) Remaining runout error measured after performing error separation on two rotations. The radius of the circle containing 90% of points is equal 42 nm—a clear improvement from the initial 1.25 μm in Fig. 4(b).

The linear drives that were used for the compensation have been tested previously and shown to be able to reach 1 nm precision in a closed-loop control with respect to the internal encoders as well as external interferometers. The mechanical imperfections of all drives lead to unintentional motions such as crosstalk and tilt, not reflected in the internal encoder readings however visible in external interferometric measurements at the reference cylinder. The measured amplitude of parasitic movements can be up to 50 nm when performing 2 μm translations, as needed for the runout corrections. However, the linear motion errors are automatically corrected, when a closed-loop control with external interferometers is employed, and have no impact on the final accuracy of the runout correction. The accuracy of the error separation depends on multiple factors, which still need thorough investigation. Improvements of the accuracy of the error separation procedure, including the better alignment of the interferometer heads would lead to the reduction of the remaining runout errors. Currently, the mutual alignment of the laser beams on the cylinder surface is done with the accuracy of about ±50 μm. We believe that this can be still improved by different techniques. Other possible factors, such as the effects of air turbulence on changes of the refractive index, can be reduced by an improved technical design of the setup.

E. Axial runout and angular wobble

So far we have shown the compensation of the radial runout using the known shape of the reference object, determined from the error separation. However, during rotation the spindle also performs parasitic movements along the axial direction, which can range up to a few micro meters. The axial runout was compensated by measuring the displacement using the vertical interferometer (Fig. 1) and correcting it using the Z linear drive. An optically flat mirror was mounted on the top of the reference cylinder. Keeping the laser spot of 3 mm in diameter at the same spot on the mirror, aligned with the rotation axis, assured that the surface roughness had no impact on the displacement measurements. The magnitude of the axial runout was reduced from ±1.8 μm down to ±2.8 nm, as achievable by the linear stages in closed-loop control. If the flatness of the mirror was a limiting factor, it is possible to characterize it using the standard optical methods, such as interferometry or by performing the error separation on a flat rotating surface, similar to the one applied to the cylindrical surface.[18,19]

Tilt of the sample due to the wobble of the rotation axis can also lead to smearing in 3D tomographic imaging. If the lateral dimensions of the sample are in the range of 10 μm, tilt by 0.2 mrad corresponds to the relative shift of the voxels on the opposite sides of the sample by 2 nm. Compensation of the tilt using a dedicated actuator can help improve the resolution even further. For this we have foreseen an additional tilt stage that will be used to correct the angular errors of the rotation axis.

IV. CONCLUSION

In this paper, we presented a method for the correction of the rotational drive errors using a non-perfect brass cylinder as a reference object. The cylinder shape was first characterized using the special measurement bench. The shape was then used together with fiber optic laser interferometers to provide feedback on the parasitic displacements that take place during rotation. As a result of such compensation, the total runout error was reduced from $\pm 1.25\ \mu$m to ± 42 nm. With this we show that the application of the error separation method allows us to use any cylindrical object as a reference surface for accurate sample positioning feedback. Moreover, we demonstrated that small, piezoelectrically driven rotation drives can potentially be used for high resolution X-ray tomography microscopes. We can see that the method for the compensation of rotational runout presented in this paper is easily scalable and could be fully integrated inside the body of the rotational drive, including the additional piezo actuators for motion corrections and interferometers for feedback. This will allow building more compact and versatile X-ray microscopes in the future, both in science and for industry.

ACKNOWLEDGMENTS

The work was done in the frame of collaboration between Max IV and Soleil synchrotron radiation facilities, funded by the Swedish research council. The authors would like to thank Ulf Johansson and Andrea Samogyi for their valuable contributions to the project.

[1] L. Li, Y. K. Chen-Wiegart, J. Wang, P. Gao, Q. Ding, Y.-S. Yu, F. Wang, J. Cabana, J. Wang, and S. Jin, Nat. Commun. **6**, 6883 (2015).
[2] I. Zanette, B. Enders, M. Dierolf, P. Thibault, R. Gradl, A. Diaz, M. Guizar-Sicairos, A. Menzel, F. Pfeiffer, and P. Zaslansky, Sci. Rep. **5**, 9210 (2015).
[3] J. N. Clark, J. Ihli, A. S. Schenk, Y.-Y. Kim, A. N. Kulak, J. M. Campbell, G. Nisbet, F. C. Meldrum, and I. K. Robinson, Nat. Mater. **14**, 780 (2015).
[4] T. Stankevič, D. Dzhigaev, Z. Bi, M. Rose, A. Shabalin, J. Reinhardt, A. Mikkelsen, L. Samuelson, G. Falkenberg, I. A. Vartanyants, and R. Feidenhans'l, Appl. Phys. Lett. **107**, 103101 (2015).
[5] M. S. Nielsen, M. B. Munk, A. Diaz, E. B. L. Pedersen, M. Holler, S. Bruns, J. Risbo, K. Mortensen, and R. Feidenhans'l, Food Struct. **7**, 21 (2016).
[6] X. Shi, P. Fischer, V. Neu, D. Elefant, J. C. T. Lee, D. A. Shapiro, M. Farmand, T. Tyliszczak, H.-W. Shiu, S. Marchesini, S. Roy, and S. D. Kevan, Appl. Phys. Lett. **108**, 94103 (2016).
[7] F. Döring, A. L. Robisch, C. Eberl, M. Osterhoff, A. Ruhlandt, T. Liese, F. Schlenkrich, S. Hoffmann, M. Bartels, T. Salditt, and H. U. Krebs, Opt. Express **21**, 19311 (2013).
[8] P. Thibault, M. Dierolf, A. Menzel, O. Bunk, C. David, and F. Pfeiffer, Science **321**, 379 (2008).
[9] M. Beckers, T. Senkbeil, T. Gorniak, K. Giewekemeyer, T. Salditt, and A. Rosenhahn, Ultramicroscopy **126**, 44 (2013).
[10] W. Xu, K. Lauer, Y. Chu, and E. Nazaretski, J. Synchrotron Radiat. **21**, 1367 (2014).
[11] J. Lim, H. Kim, and S. Y. Park, J. Synchrotron Radiat. **21**, 827 (2014).
[12] M. Holler, J. Raabe, A. Diaz, M. Guizar-Sicairos, C. Quitmann, A. Menzel, and O. Bunk, Rev. Sci. Instrum. **83**, 73703 (2012).
[13] E. Nazaretski, K. Lauer, H. Yan, N. Bouet, J. Zhou, R. Conley, X. Huang, W. Xu, M. Lu, K. Gofron, S. Kalbfleisch, U. Wagner, C. Rau, and Y. S. Chu, J. Synchrotron Radiat. **22**, 336 (2015).
[14] G. Martínez-Criado, J. Villanova, R. Tucoulou, D. Salomon, J.-P. Suuronen, S. Labouré, C. Guilloud, V. Valls, R. Barrett, E. Gagliardini, Y. Dabin, R. Baker, S. Bohic, C. Cohen, and J. Morse, J. Synchrotron Radiat. **23**, 344 (2016).
[15] J. Wang, Y. C. Karen Chen, Q. Yuan, A. Tkachuk, C. Erdonmez, B. Hornberger, and M. Feser, Appl. Phys. Lett. **100**, 143107 (2012).
[16] M. Holler, A. Diaz, M. Guizar-Sicairos, P. Karvinen, E. Färm, E. Härkönen, M. Ritala, A. Menzel, J. Raabe, and O. Bunk, Sci. Rep. **4**, 3857 (2014).
[17] S. Kubsky, A. Lestrade, N. Jobert, C. Engblom, and F. Alves, EU patent application No PCT/EP2015/074011 (26 May 2016).
[18] R. Grejda, E. Marsh, and R. Vallance, Precis. Eng. **29**, 113 (2005).
[19] E. Marsh, J. Couey, and R. Vallance, J. Manuf. Sci. Eng. **128**, 180 (2006).
[20] M. J. Jansen, P. H. J. Schellekens, and B. De Veer, "Advanced Spindle Runout-Roundness Separation Method" in *Advanced Mathematical and Computational Tools in Metrology V*, Series on Advances in Mathematics for Applied Sciences: Vol. 57 (World Scientific, Singapore, 2001) pp. 212–219.